RL-TR-93-165
In-House Report
September 1993

AD-A274 002

# COMPONENT CHARACTERIZATION AND DEVELOPMENT II

Jacqueline D. Smith

DTIC
ELECTE
DEC 2 2 1993
S E D

*APPROVED FOR PUBLIC RELEASE; DISTRIBUTION UNLIMITED.*

93-30834

**Rome Laboratory
Air Force Materiel Command
Griffiss Air Force Base, New York**

93 12 21 174

This report has been reviewed by the Rome Laboratory Public Affairs Office (PA) and is releasable to the National Technical Information Service (NTIS). At NTIS it will be releasable to the general public, including foreign nations.
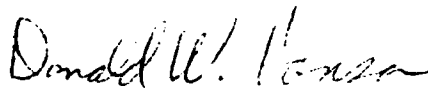
RL-TR-93-165 has been reviewed and is approved for publication.

APPROVED:

JAMES W. CUSACK, Chief
Photonics & Optics Division
Surveillance & Photonics Directorate

FOR THE COMMANDER:

DONALD W. HANSON, Director
Surveillance & Photonics Directorate

If your address has changed or if you wish to be removed from the Rome Laboratory mailing list, or if the addressee is no longer employed by your organization, please notify RL (OCPA) Griffiss AFB NY 13441-5700. This will assist us in maintaining a current mailing list.

Do not return copies of this report unless contractual obligations or notices on a specific document require that it be returned.

# REPORT DOCUMENTATION PAGE

Form Approved
OMB No. 0704-0188

| 1. AGENCY USE ONLY (Leave Blank) | 2. REPORT DATE | 3. REPORT TYPE AND DATES COVERED |
|---|---|---|
| | September 1993 | In-House    Oct 91 - Dec 92 |

| 4. TITLE AND SUBTITLE | 5. FUNDING NUMBERS |
|---|---|
| COMPONENT CHARACTERIZATION AND DEVELOPMENT II | PE - 62702F<br>PR - 4600<br>TA - P2<br>WU - 08 |
| **6. AUTHOR(S)**<br>Jacqueline D. Smith | |

| 7. PERFORMING ORGANIZATION NAME(S) AND ADDRESS(ES) | 8. PERFORMING ORGANIZATION REPORT NUMBER |
|---|---|
| Rome Laboratory (OCPA)<br>25 Electronic Pky<br>Griffiss AFB NY 13441-4515 | RL-TR-93-165 |

| 9. SPONSORING/MONITORING AGENCY NAME(S) AND ADDRESS(ES) | 10. SPONSORING/MONITORING AGENCY REPORT NUMBER |
|---|---|
| Rome Laboratory (OCPA)<br>25 Electronic Pky<br>Griffiss AFB NY 13441-4515 | |

**11. SUPPLEMENTARY NOTES**

Rome Laboratory Project Engineer:   Jacqueline D. Smith/OCPA (315) 330-3063

| 12a. DISTRIBUTION/AVAILABILITY STATEMENT | 12b. DISTRIBUTION CODE |
|---|---|
| Approved for public release; distribution unlimited. | |

**13. ABSTRACT (Maximum 200 words)**

The effort entitled, "Component Characterization and Development II" was established in the Rome Lab Photonics Center Analog & Lightwave Photonics Branch as part of the overall in-house program plan to advanced the state-of-the-art in optics and electro-optics.  The objective of the effort is to specify, acquire, and/or develop components for Air Force Command, Control, Communications, and Intelligence (C3I) applications. The source of prototype devices was designated to include academia, industry, and government organizations.  Actual performance data was measured for both electro-optic and fiber-optic based devices that were of interest to communications, spatial laser control, and optical beamforming applications.  Additionally, several novel approaches to device fabrication were investigated through a BAA contract with Syracuse University.

| 14. SUBJECT TERMS | | 15. NUMBER OF PAGES |
|---|---|---|
| electro-optics, prototype devices, spatial laser control, communications | | 48 |
| | | 16. PRICE CODE |

| 17. SECURITY CLASSIFICATION OF REPORT | 18. SECURITY CLASSIFICATION OF THIS PAGE | 19. SECURITY CLASSIFICATION OF ABSTRACT | 20. LIMITATION OF ABSTRACT |
|---|---|---|---|
| UNCLASSIFIED | UNCLASSIFIED | UNCLASSIFIED | U/L |

# Table of Contents

| Accesion For | | |
|---|---|---|
| NTIS CRA&I | | ☒ |
| DTIC TAB | | ☐ |
| Unannounced | | ☐ |
| Justification | | |
| By | | |
| Distribution / | | |
| Availability Codes | | |
| Dist | Avail and/or special | |
| A-1 | | |

DTIC QUALITY INSPECTED 3

## List of Figures

## List of Tables

## Acknowledgments

## List of Symbols, Abbreviations, and Acronyms

| | |
|---|---|
| **ALDOP** | Artificial Long Delay Optical Processor |
| **AO** | acousto-optic |
| **BAA** | Broad Agency Announcement |
| **C$^3$I** | Command, Control, Communications, & Intelligence |
| **CdTe** | cadmium telluride |
| **FLC** | Ferroelectric Liquid Crystal |
| **InSb** | indium antimonide |
| **JON** | job order number |
| **$\lambda_\tau$** | target operating wavelength $\lambda$ |
| **LPM** | Laboratory Program Manager |
| **$\mu$m** | unit of light wavelength, 1 micrometer $= 1 \times 10^{-6}$ meter |
| **PATT** | Photon Assisted Tunneling Transistor |
| **pixel** | picture element |
| **ps** | $1 \times 10^{-12}$ second |
| **SLM** | Spatial Light Modulator |

**Preface**

The more significant results of this effort were published papers in conference proceedings or published in interim technical reports. The organizational chain for referenced publications is through the Air Force Materiel Command (AFMC), Rome Laboratory Photonics Center , Analog & Lightwave Photonics Branch, in-house effort entitled 'Component Characterization & Development' (JON 4600P208). This report covers the work performed from October 1991 until the project was canceled in December 1992.

# Introduction

The effort entitled "Component Characterization and Development" was established in the Analog & Lightwave Photonics Branch as part of the overall in-house program plan to advance the state-of-the-art in optics and electro-optics. The objective of the effort was to specify, acquire, and/or develop components for Air Force Command, Control, Communications, and Intelligence ($C^3I$) applications. The source of prototype devices was designated to include academia, industry, and government organizations. The ability of this effort to provide supporting and in-situ data has proven to be of great value to both prototype and ready-for-market device designers.

Actual performance data was measured for both electro-optic and fiber-optic based devices that were of interest to communications, spatial laser control, and optical beamforming applications.

# CdTe-InSb Nonlinear Etalon Switch [1]

The switching response of a CdTe-InSb nonlinear etalon subject to an intense light beam is reported. The device is illuminated with a high intensity pulsed pump beam and a low intensity pulsed probe beam. The pump beam has a wavelength $\lambda$ that corresponds to a negative slope of the low intensity reflectance spectrum of the etalon and has sufficient power to change the index of refraction in the etalon cavity. This causes a shift of the spectrum, a decrease in the reflectivity, and an increase in the electric field in the etalon cavity which further shifts the spectrum. This process continues until a minimum reflection level is reached. The output yields the convolution of the probe beam with the device response to the pump pulse. It appears that the switching response of the etalon is much faster than could be determined with the 100 ps pulses used.

Etalons containing non-linear optical materials have recently been used in optical switches[2,3]. The switching response of a CdTe-InSb nonlinear etalon subject to an intense pulsed light beam is reported. The devices consist of a 0.45 $\mu$m thick epitaxially grown CdTe film on an InSb substrate. The InSb substrate has a reflectivity similar to metals at room temperature. The transparent CdTe film and the reflecting InSb substrate form an optical resonant cavity. The device thickness was optimized for operation at the target wavelength $\lambda_\tau$= 1.064 $\mu$m.

The normalized low light intensity spectral response of the reflection coefficient (Figure 1) was obtained by using a white light source and an optical spectrum analyzer. The broadband spectral response of the optical components used to transmit and focus the white light was used as the normalization factor. The approximate location of $\lambda_\tau$ is indicated by the arrow graphic.

Note that for wavelengths $\lambda < \lambda_{Eg}$ ($\lambda_{Eg}$ = 816 nm) corresponding to the energy gap of CdTe, there is substantial loss. For $\lambda > \lambda_{Eg}$ large resonant excursions are observed. Observe that the slope of the reflectance spectrum is negative at $\lambda_\tau$. Operating the device at a wavelength longer than $\lambda_{Eg}$ also minimizes thermal effects. Thermal effects often mask the theoretical fast

response of etalon switches based on optical non-linearities involving conduction electrons[4,5]. No thermal effects were observed in our experiments.
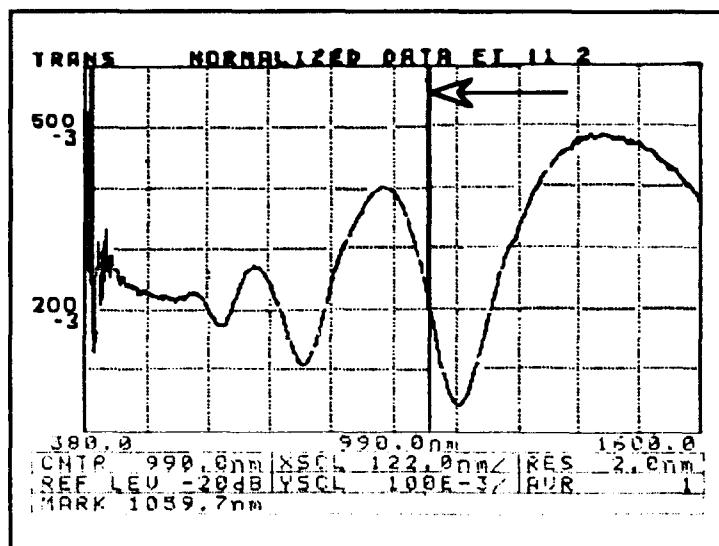


Figure 1. Low light intensity spectral response of the etalon.

A mode-locked Nd:YAG laser with 3 Watts average power, a pulse width of 100 ps at the half maximum point and pulse repetition rate of 100 MHz was used to test the switching of the etalon. The laser was initially attenuated and split into a 94:6 pump to probe beam power ratio. The probe beam passed through a variable delay arrangement using a motorized linear translation stage and a retroreflector. The relative arrival times at the etalon of the pump and probe beams could be varied so that the probe preceded the pump, or vice versa. The probe and pump beams were orthogonally polarized.

The pump beam was focused through a 20X microscope objective at normal incidence onto the etalon device. The probe beam was incident at 45° to the plane of the device, reflected from the device and focused on a silicon (Si) photodetector. The pump beam was chopped at a 1000 Hz rate to compensate for the comparatively slow response of the Si photodetector. The output of the photodetector and a reference signal obtained from the chopper were applied to a lock-in amplifier. Before taking data it was ascertained that there was no output from the lock-in amplifier if either the probe or pump beam was blocked.

The output is obtained by sweeping the probe pulse past the device response to the pump pulse. This output yields the convolution of the probe beam with the device response to the pump pulse. A typical normalized output response of the reflectivity of the device is shown in Figure 2.
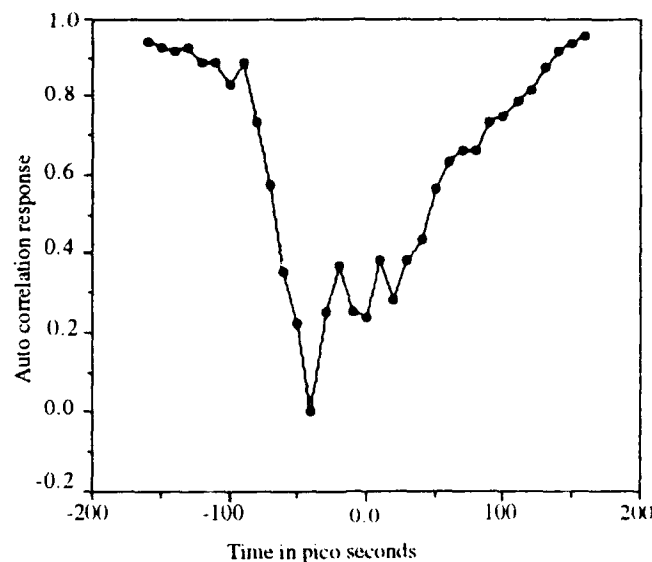


Figure 2. Normalized reflection response of the etalon.

We interpret the output as follows: The electric field of the pump beam changes the index of refraction of the CdTe layer shifting the spectral response (Figure 1 ) to higher wavelengths, resulting in a decrease in reflectivity at $\lambda_\tau$. However, the pump beam increases the electric field in the cavity which causes more light to be absorbed in the CdTe film. This, in turn, causes a further shift in the spectrum to higher wavelengths, a further decrease in the reflectivity, and an increase in the electric field in the cavity. The process continues until a minimum reflectivity is reached (see Figure 2). During the fall time of the pump pulse this process is reversed and the reflected probe light intensity increases.

The characteristics of the output pulse is dependent on the convolution of the probe with the device response to the pump. For ideal Gaussian pump and probe pulses and no delay in the device, the output pulse should have a half height pulse width equal to $\sqrt{2}$ times the half height pulse width of the original pulses. Neither the probe nor the pump beams were Gaussian. The pump and probe pulses had a half height pulsewidth of about 100 ps. The

8

device response has a half height (at 0.5 in Figure 2) pulse width of about 110 ps. The short output response can be attributed to the fact that the modulation of the etalon resonance does not start until a certain amplitude of the pump pulse is reached. The half height pulsewidth using the modulation threshold of the pump beam as a base line is narrower than 100 ps. Nevertheless, it appears that the response of the etalon is much faster than can be determined with the 100 ps pulses. Future experiments with a shorter pulse width laser will be performed to measure the exact switching speed of the CdTe-InSb etalon.

## 100 Element Ferroelectric Liquid Crystal Spatial Light Modulator [6]

A Spatial Light Modulator (SLM) is a device designed for computer controlled modulation of laser light on an individual element, or pixel, basis. SLM fabrication is conventionally done in two-dimensional arrays to provide sufficient area to cover typical laser beam dimensions (on the order of $mm^2$). The interest in investigating a spatial light modulator was to determine the feasibility of its use in controlling the throughput of pixels generated by a binary phase grating element that splits an incoming laser beam into twenty-five (25) spatially separated beams. For this purpose, a custom made Ferroelectric Liquid Crystal (FLC) spatial light modulator was tested to determine its contrast ratios for multi-element and single element areas.

The technical report entitled "Measurement of Contrast Ratios for a Ferroelectric Liquid Crystal Spatial Light Modulator" (# RL-TR-91-404 )[7] describes the software and commands used to control the device, the experimental methods implemented to study the device, and the experimental results. Portions of that report are repeated here for illustration purposes. The SLM was returned to Displaytech, Inc., of Boulder, Colorado, in August 1991 to repair the switching malfunction that was discovered in one bank of the DDR128 Driver. Displaytech confirmed that one bank failed to switch between its two output levels and malfunctioned by delivering a constant voltage. The device was repaired and returned in May 1992. The lengthy repair time resulted from a catastrophic failure of the device during the repair. Electrochemical potentials being generated in the device had induced breaking in the transparent ITO

electrodes on the glass surface. In addition, the ITO adhesion was poor. These problems resulted in the failure of the device during repair of the driving circuitry.

Upon the return of the SLM and its driver, the device was tested at 1320 nm to determine its uniformity and overall extinction ratio. We sought to characterize this device's operating capability at 1320 nm by investigating the uniformity of individual elements and contrasting the results with that of the device as a whole. The data was also compared to a theoretical determination of the array's output.

The primary component of the SLM consists of an array that is comprised of two glass plates separated by a thin film of liquid crystal material. A reflective chromium mask creates 100 liquid crystal elements (pixels) in a 10x10 array pattern. Transparent electrical contacts are deposited on the plates to provide the patterned and common electrodes for DC biasing. By applying a voltage across the contacts, an electric field is produced which induces the molecules in the liquid crystal to orient themselves in one of two preferred states that differ in alignment by 45 degrees. The state with which the molecules choose to align can be changed by switching the polarity of the electrical contacts.

The array is implemented in a spatial light modulation system when it is illuminated with a coherent source, inserted between crossed linear polarizers, and has its contact switching controlled by a computer (see Figure 3). If polarized light is incident on the array when the molecules in a liquid crystal element are aligned, the element functions as a half-wave plate. A half-wave plate rotates the polarization of the incident light through an angle twice that formed by the incoming polarization vector and the molecular state of orientation (optic axis). When an element is illuminated with light polarized parallel to the optic axis, no rotation in the polarization of the light occurs in the throughput. In this case, the analyzer minimizes transmission through the system, since its transmission axis is perpendicular to both the input polarization and optic axis (see Figure 3, CLOSED state).

Applying the opposite voltage to the contacts results in rotating the element's optic axis $45^\circ$ with respect to its original orientation. The light transmitted through the array therefore undergoes a $90^\circ$ rotation in

polarization. Consequently, its polarization is parallel to the transmission axis of the analyzer and results in maximum transmission (see Figure 3, OPEN state). The pattern of light transmitted through the array can thus be regulated by controlling the voltages sent to each element.



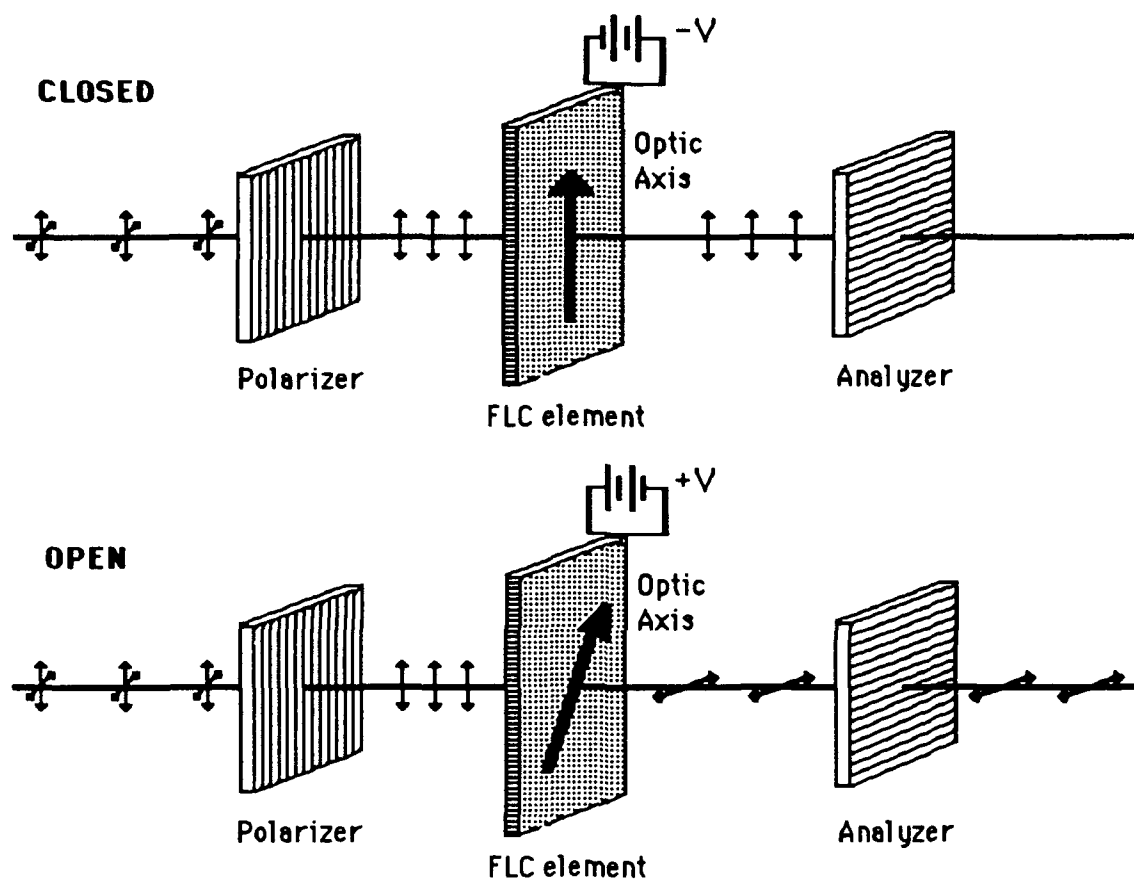Figure 3. Operating Principles of SLM

## Experimental Method

Before reactivating the device, the pins on each bank of the DDR128 Driver were tested to confirm that each channel delivered +/- 17 V when the driver was programmed to switch the entire array on and off. Table 1 below lists the range of measured voltages recorded for each back of the DDR128 Driver when programmed to continuously switch the SLM.

11

| Driver bank | Maximum voltage | Minimum voltage |
|:-----------:|:---------------:|:---------------:|
| A | 15.85 - 16.19 V | -15.88 - -16.20 V |
| B | 15.93 - 16.09 V | -15.95 - -16.11 V |
| C | 16.00 - 16.12 V | -16.00 - -16.13 V |
| D | 16.00 - 16.17 V | -16.00 - -16.18 V |

Table 1.   Range of output voltages by DDR128 Driver banks.

The optical setup for power measurements of multiple areas on the SLM is shown in Figure 4a. The modified system for measuring the light transmission of a single pixel is shown in Figure 4b. The spatial filter assembly (15x objective, pin hole, and collimating lens) was eliminated for the single case in order to obtain the spot size needed to illuminate only one pixel of the SLM. The optical power incident on the array for the single pixel case was controlled by adding more neutral density filters at the left side of the system.

A 75 mW Amoco laser that operated at λ = 1318.7 nm was used as the light source. The laser supplied linearly polarized light at a ratio on the order of 500:1. A Newport modular beam-expanding filter was used to produce a collimated beam that would uniformly illuminate the active area of the SLM. Both the SLM and the analyzer were mounted on rotation stages that were centered to rotate about the beam axis. The light throughput from this system was focused onto a Newport Optical Power Meter for transmission tests or cast onto a screen for viewing through a lead-selenide CCD camera.

For investigating a single element of the SLM, a variable neutral density filter was inserted between the laser and the spatial filter to attenuate the beam (note that the maximum power that should be incident on the SLM is 5 mW/mm$^2$). In addition, a mask was introduced to assure that each element would be illuminated by the same portion of the collimated beam. The

unmasked portion of the beam was then focused onto the element of interest. Verification of the element's location in the array was determined by the projection of its output onto a screen and subsequent viewing using the CCD camera.
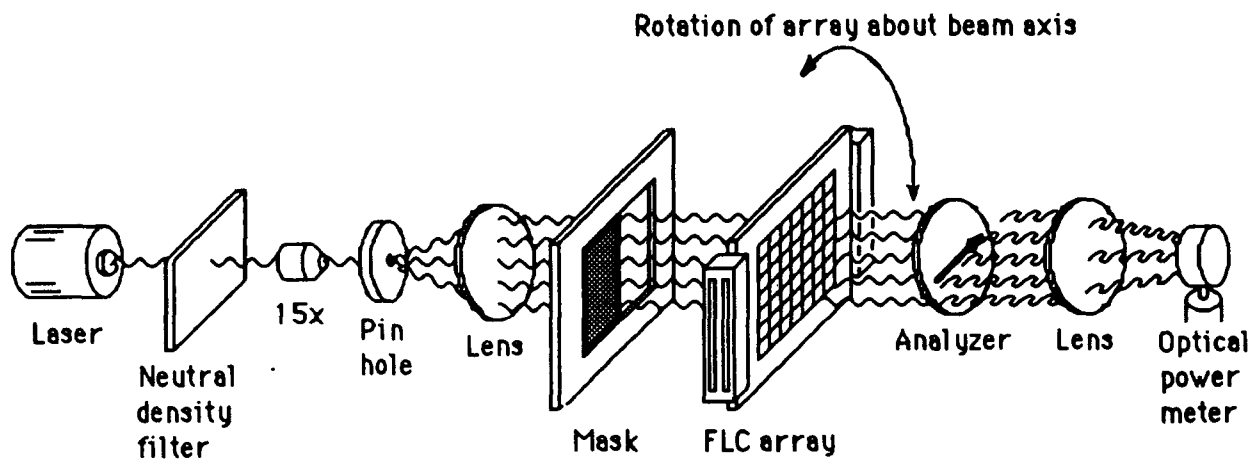
Figure 4a. Experimental setup for power measurements of multiple pixels
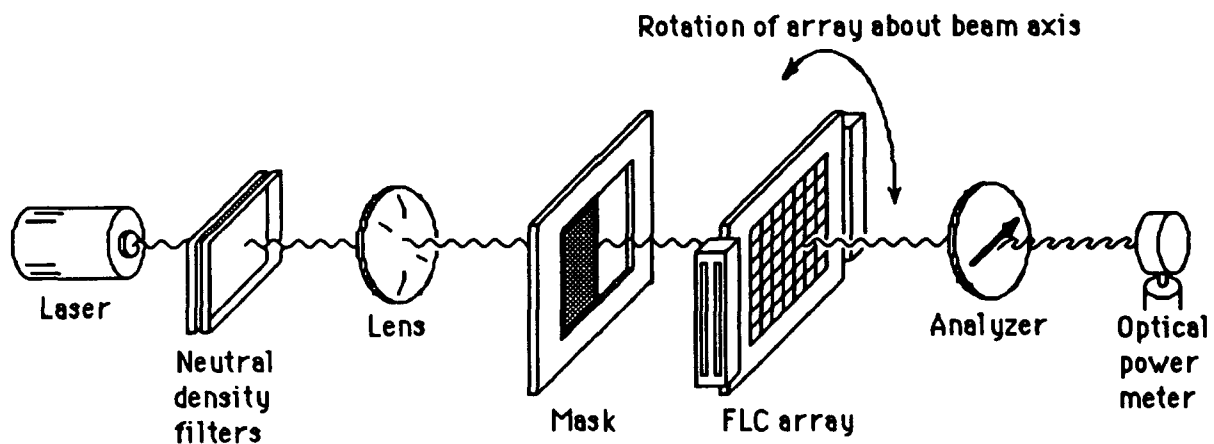
Figure 4b. Experimental setup for power measurements of a single pixel

## Experimental Results

The extinction ratio of the entire array was tested at two different power levels. The input polarization was measured to be approximately 2 degrees

and the SLM was oriented at 7.9 degrees below the horizontal. Table 2 below lists the analyzer position yielding the largest extinction ratio for the two tests. The ratio was relatively unchanged, even though the input power for one sampling was almost twice that of the other. The graphs of output versus analyzer angle show how the throughput depended on the analyzer's

| Incident power | Analyzer angle | Power (in μW) Maximum | Minimum | Extinction ratio |
|---|---|---|---|---|
| ≥ 655.0 μW | 93° | 353.9 | 8.1 | 43.7 |
| ≥350.8 μW | 92° | 278.9 | 6.5 | 42.9 |

Table 2. Extinction ratios of entire SLM array at 1320 nm

orientation. These graphs demonstrate how the entire SLM did not function as a perfect half-wave plate.

To determine how the overall extinction ratio was dependent on the individual elements, the throughputs of six elements were tested for their dependence on the analyzer position. The input polarization was measured to be at 1.5 degrees and the SLM was oriented at 0 degrees for all six tests. Table 3 lists the extinction ratios of the six elements at the analyzer settings near and at throughput maxima. Note that for these six elements, there was little variation in the optimal analyzer orientation; the adjustments needed to maximize the throughput were within a degree.

In addition, note that if one corrected for 7.9 degree difference in the SLM orientation that existed for the global test, the location of the throughput maximum would also have been near 100 degrees. The dependence of the output on analyzer position for each of the tested elements is revealed in the

graphs for individual pixels. The pixels also do not act as perfect half-wave plates when considered separately. The global problem apparently does not result from individual elements behaving as half-wave plates with different optic axes, but from each element not switching its optic axis by 45 degrees. From the graphs, the switching of the optic axis appears only to be 27 degrees.

| Analyzer angle | Extinction ratio for the element n,m=( x : 1) @ 1320 nm | | | | | |
| --- | --- | --- | --- | --- | --- | --- |
| | 6,2 | 6,4 | 6,6 | 6,8 | 8,3 | 8,5 |
| 100° | 96.2 | 85.0 | 102.4 | 79.9 | 116.6 | 80.1 |
| 101° | 103.2 | 90.3 | 112.5 | 81.6 | 111.7 | 81.6 |
| 280° | 83.5 | 67.9 | 109.2 | 68.0 | 94.6 | 69.7 |
| 281° | 88.6 | 68.8 | 111.2 | 69.3 | 107.2 | 77.4 |

Table 3. Extinction ratios for various SLM elements

A confirmation of the results was determined by fitting the data from one of the elements (6,6) to a theoretical determination of the power output that would be seen through the analyzer. If we assume that the light incident on the analyzer propagates in the z-direction and its electric field consists of the following x- and y- components after passing through the SLM in one of its switching states:

$$\mathbf{E} = \mathbf{i}\, E_o\, \cos \alpha \cos \omega t + \mathbf{j}\, E_o \sin \alpha \cos (\omega t + \phi)$$

where $\alpha$ is the angle the incident polarized light makes with the optic axis and $\phi$ is the phase shift in the y-component introduced by the SLM, then the resulting power that will be read by the optical power meter can be calculated by the following relation.

$$P = ( (i \, E \, \cos \alpha \, \cos \omega t + j \, E \, \sin \alpha \, \cos (\omega t + \phi)) \; (i \, \cos \theta + j \, \sin \theta) )^2$$

where $\theta$ is the analyzer angular position and the expression $(i \, \cos \theta + j \, \sin \theta)$ is the rotational operator on the power **P**. Simplifying this equation, taking into account that the power meter can only measure time average responses, yields:

$$P = ( c \, E^2 \, (1 + \cos 2\alpha \, \cos 2\theta + \sin 2\alpha \, \sin 2\theta \, \cos \phi )$$

If we consider the SLM in its other switched state, i.e. we introduce rotation $\delta$ in the optic axis, the light passing through the SLM will undergo a rotation of $2\delta$. In that case, the power read by the meter will be:

$$P_{switch} = ( c \, E^2 \, (1 + \cos 2(\alpha + 2\delta) \, \cos 2\theta + \sin 2(\alpha + 2\delta) \, \sin 2\theta \, \cos (\phi + 2\delta) )$$

For the case of element 6,6, by choosing $\alpha = 10$ degrees, $\phi = 12$ degrees, $\delta = -28$ degrees, and adjusting the amplitude, the graphs of the theoretical output are produced. Comparison with the graph of the data obtained for element 6,6 shows that this calculation accurately predicts the measured data. Similar fits could be made for the other elements and the entire array in order to determine the rotation of the optic axis induced by the switching voltage and the phase shift occurring in the beam that results from its passage through the SLM.

## Aluminum Oxide Tunneling AND Gate [8]

### Tunneling Junction

We have fabricated and tested several photon assisted tunneling diodes. The devices consisted of a 0.5 mm wide aluminum strip vacuum deposited on a glass substrate. The aluminum strip was deposited through a mask. The aluminum film was oxidized in ambient air. Silicon oxide (SiO) insulating edge protection layers were deposited through a mask onto the edges of the aluminum strip.
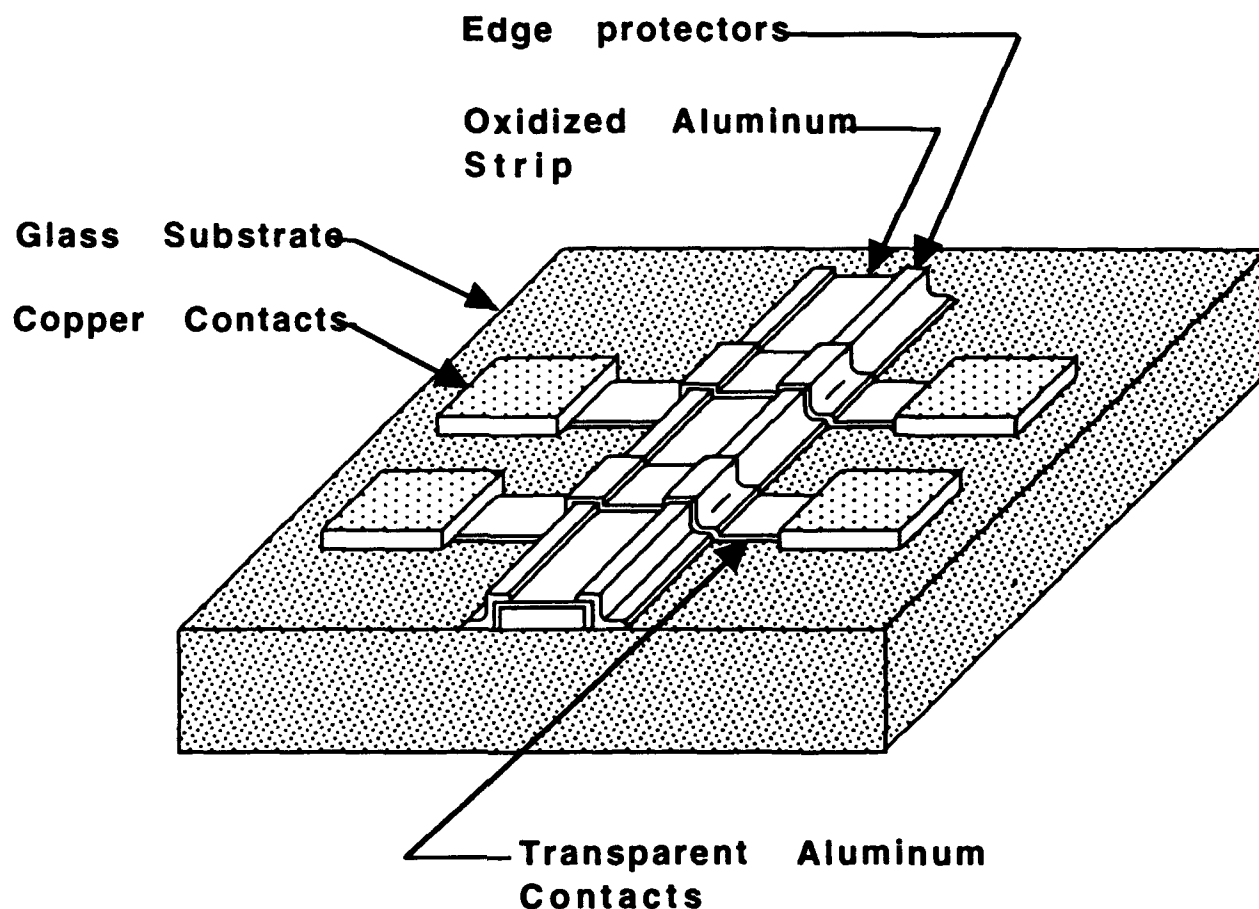
Edge protectors

Oxidized Aluminum Strip

Glass Substrate

Copper Contacts

Transparent Aluminum Contacts

Figure 5. Tunneling diodes structure.

Thin strips (80 Å) of aluminum were vacuum deposited across the oxidized aluminum strip with edge protectors as shown in Figure 5. These top aluminum contacts are thin enough to be transparent to light. Copper contacts were deposited on the thin aluminum strips on either side of the oxidized aluminum strip.

The edge protection prevents shorting at the edges of the bottom aluminum strip. We measured the tunneling current. All tunneling currents measured were of the order of a few microamperes. These values are too low for practical applications. The oxide layers on all devices fabricated were much too thick causing very low values of tunneling currents. However, we were able to observe an increase in the tunneling current by about 5% with illumination from a HeNe laser. The signals obtained were rather small. The reason for this is that 98% of the light is reflected and only 2% is absorbed by the device and that the oxide layer was very thick. The light absorption can greatly be increased by using an anti-reflection coating. Since the device is made out of a metal a standard anti-reflection coating could not be used. However, an etalon consisting of a thin transparent film polystyrene layer coated with a 50Å aluminum layer was tried. Light absorption increased by a factor of about ten with the use of the etalon. However, the thick oxide layer still limited the tunneling current.

The energy diagram of the tunnel barrier is shown in Figure 6. The barrier potential at a metal insulator junction actually extends into the insulator beyond the metal. The barrier potential is equal to the energy required to remove an electron from the metal. Since a metal acts as a very good mirror for electromagnetic phenomena, including light, the electron that is being removed from the metal experiences a force due to an effective image charge in the metal. The potential energy of the electron, due to the image charge, increases with distance from the metal as is illustrated by the solid potential barrier curve near each metal in Figure 6. The overlap of these potential barrier curves from both metals form the actual potential barrier of the tunnel junction.
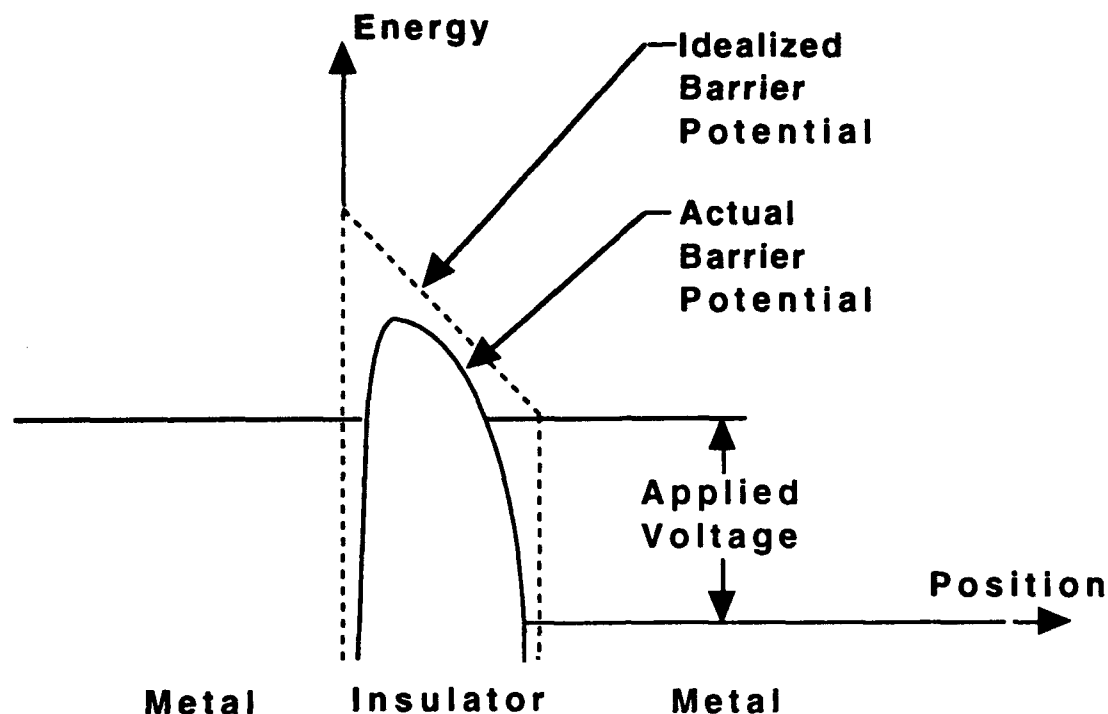
Figure 6. Metal-Insulator-Metal tunnel junction.

## Photon Assisted Tunneling Transistor

Since the late 1950s various attempts have been made to fabricate Tunneling Transistors. This device consists of a thick metal emitter, a 30 - 50Å thick insulating oxide layer, a thin (20 - 100 Å thick) metal base, another 30 - 50 Å thick insulating oxide layer, and a metal collector electrode. This is a Metal, Oxide, Metal, Oxide, Metal (MOMOM) device. Such a device could be very fast since the quantum mechanical tunneling process is very fast. The quantum mechanical tunneling current can theoretically be switched in a few fsec. However, capacitive effects will limit the speed of a practical device. To date no successful MOMOM transistor has been built. The reason these devices did not work is that if the metal film that forms the base is thick enough to conduct horizontally, it will be too thick for electrons to penetrate the film from insulator to

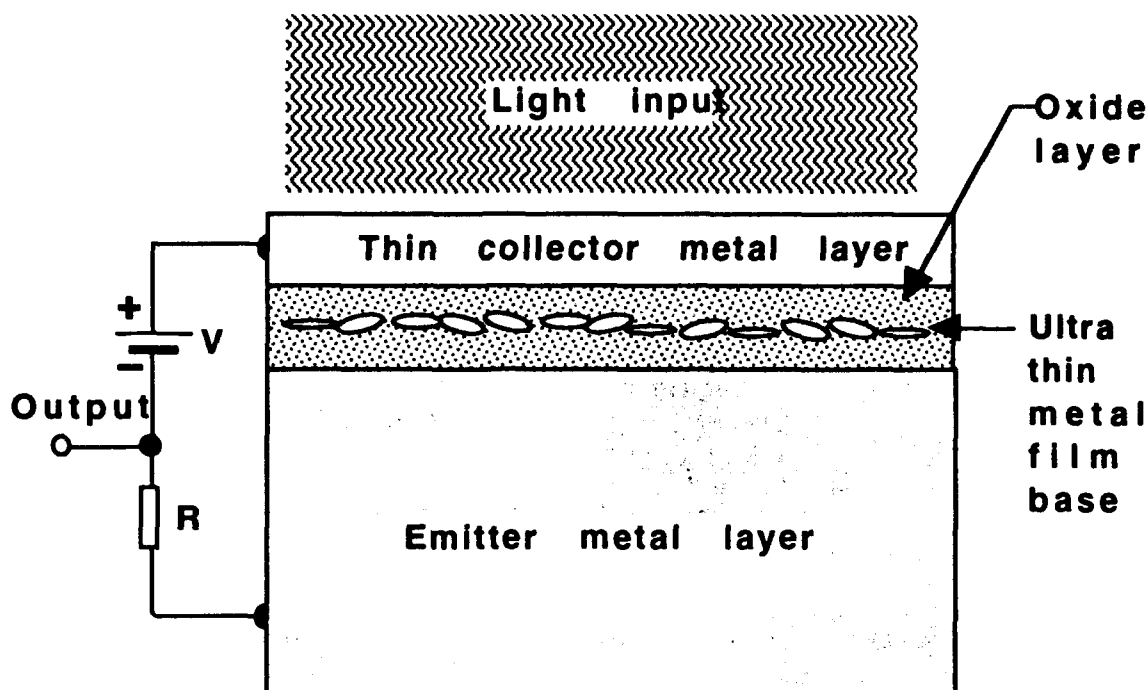Figure 7. Schematic of a Photon Assisted Tunneling Transistor (PATT).

insulator. The electrons are scattered in the metal. It is possible to make very thin metal base layers (10-20 Å), however, such layers don't conduct horizontally.

As an alternative to the diode structure, we plan to build MOMOM devices with exceedingly thin metal base layers only 10 - 20 Å thick. We plan to access these layers optically through a thin (100 Å thick) collector electrode rather than trying to make electrical contact to them. The bottom emitter electrode is made out of a different metal than the base and collector electrodes. This generates a built-in potential difference between the emitter and base electrodes. When such a junction is illuminated, an additional photovoltage is developed between the emitter and base electrodes. This photovoltage can be used to control the tunneling current from emitter through the ultra thin base to the collector. We are still hoping to try to build a Photon Assisted Tunneling Transistor (PATT). Two of these devices can be connected in

20

series to form a Photon Assisted Tunneling AND Gate. This work is being continued under another in-house effort (JON 4600P206), Optical Interconnects.

## Laser Beam Analysis System

The design, specification, and procurement of the Laser Beam Analysis System (LBAS) has created a state-of-the-art image capture and processing. The system was designed and assembled by J. D. Smith with technical assistance from Mr. Wesley Foor.

The system consists of a lead selenide camera with visible to near-IR sensitivity whose video output is fed into a Quadra 900 computer via a NTSC/RS170 compatible video frame grabber. The capabilities of the LBAS include rudimentary laser beam profiling, surface analysis of optical elements through relative measurement techniques, and optimization of optical alignment. The camera is sensitive in the regions above that of CCDs, namely 1.0 $\mu$m. The LBAS is limited to use in low power (< 1000 $\mu$W/cm$^2$), continuous wave (CW), visible to near-IR ($\lambda \leq 2.1$ $\mu$m) wavelengths. Affordable commercial beam profiler systems are limited with respect to post-image capture processing and flexibility of analysis. The system was delivered in March 1992, with minor CPU RAM upgrades to enhance the run-time performance of the system.

The complete system capability has provided image capture and analysis for the FLC SLM experiments described in this report. The system played a key role in a project involving surface analysis of optical coatings subjected to micrometeor impacts while onboard a communications satellite. The system will continue to be used for tasks affiliated with Automated Optical Target Recognition and will continue to be improved in coming fiscal years.

# Optical Waveguides and Waveguide Lasers

## Planar and Ridge Waveguides

We fabricated two types of waveguides: planar and ridge. Planar waveguides are constructed by doping channels in a glass substrate just below the surface as shown in Figure 8a. Ridge waveguides have channels of doped glass that protrude above the substrate surface. Planar waveguides can only guide light around small curvatures, typically about 10 cm in radius. Ridge waveguides can guide light around substantially smaller radii of only a few millimeters. The light input and output to all waveguides is via single mode fibers. Indeed, all tests to date on the waveguides were performed using light coupled into the waveguides through a single mode fiber.
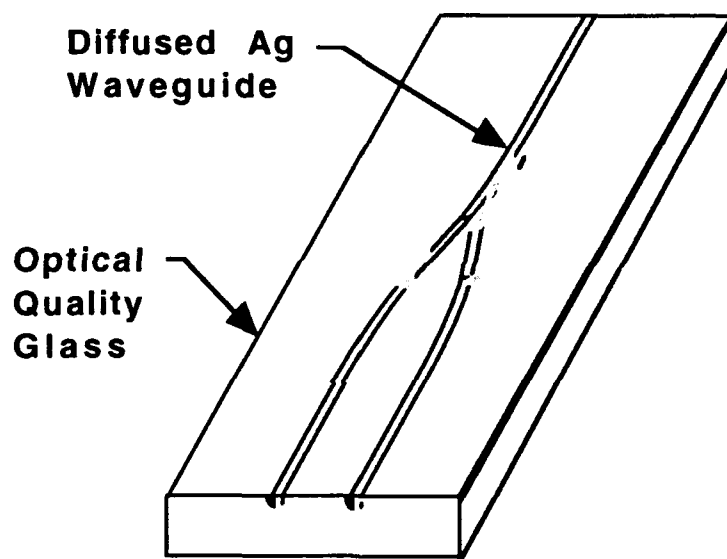
**Diffused Ag Waveguide**

**Optical Quality Glass**
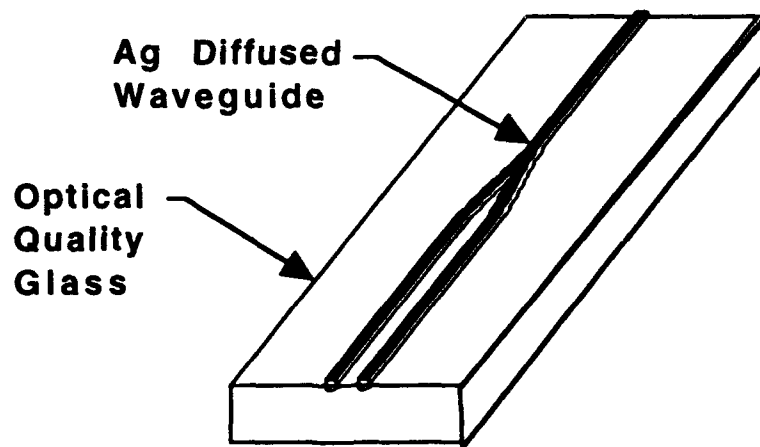
Figure 8a. Planar waveguide.

Figure 8b   Ridge waveguide.

## Waveguide Application

Optical waveguides have many applications including pulse multiplexing and demultiplexing networks. A multiplexing network consists of a single input waveguide that branches into a number of waveguides. Each waveguide branch has a different optical path length. The waveguides are then recombined. The differences in the optical path length are integer multiples of the shortest path length difference. Consider a pulsed optical signal with a repetition rate longer than the longest difference in optical delay. Each path delays the pulse by a different time interval. When the delayed pulses are recombined, a signal with a much higher pulse repetition rate results. The realization using a single glass substrate results in the construction of precise delays. Also, since all the delay elements are located on the same substrate, they expand and contract with temperature uniformly.

However, to make such a device useful, the pulses have to be not only delayed but also modulated. Therefore, each path must also contain a modulator capable of switching the pulse that runs through the particular waveguide guide on and off. These modulators can be fabricated by either depositing ZnO on the waveguide and patterning the ZnO into a Mach-Zehnder interferometer modulator configuration or attaching a $LiNbO_3$ Mach-Zehnder modulator onto the waveguide. Since both $LiNbO_3$ and ZnO have

substantially higher indices of refraction than glass, the light will switch from the glass into the ZnO or LiNbO$_3$.

## Waveguide Fabrication

The waveguide is fabricated by doping channels in the surface of optical quality glass with silver. Silver increases the index of refraction of the glass. Thus, light will be confined to the doped channels in the glass. Since the increase of the index of refraction in the waveguide region is small, only about 0.1% to 0.05%, the light will be weakly guided. This restricts the curvature of the guides to large radii. On the other hand, since there are large regions on the sides of the waveguides where the light intensity decreases exponentially, it is easy to construct evanescently coupled waveguides.

The doping was accomplished as follows: a chromium metal film was vacuum deposited on the glass substrate. A layer of photoresist was deposited on the chromium film. The photoresist was exposed through a mask and developed. This left photoresist everywhere except where the waveguide would be. The chromium film was next etched away from the waveguide pattern. Next a silver metal film was vacuum deposited on the chromium film leaving the silver film in contact with the substrate where the waveguide would be. Finally, chromium metal films were vacuum deposited both on the top and bottom of the glass substrate with the top chromium film covering the silver film. Electrodes were attached to the chromium films. A voltage of about 10 Volts was applied between the chromium film electrodes while the substrate was heated to 350 °C for 2 hours. During this process the silver diffused into the glass forming a channel with a higher index of refraction than the surrounding glass. This process is known as electric field assisted diffusion. After the diffusion process was completed the chromium film was etched off resulting in a planar waveguide.

Ridge waveguides are made by first fabricating a planar waveguide. Photoresist is, again, deposited on the glass substrate. The photoresist is exposed through a mask covering the waveguide, and developed. The mask is aligned with the waveguide using alignment marks. This leaves photoresist on the waveguide. The glass substrate is etched using HCl in H$_2$O in

a 1:4 ratio for one hour. This is followed by etching in a 1:15 HCl solution in $H_2O$ for 5 minutes to smooth the waveguide edges. Lastly, the remaining photoresist is removed leaving an elevated ridge waveguide on the glass substrate. The air boundary of the ridge waveguide in conjunction with the silver doping provides stronger guiding than is possible in a planar waveguide. The ridge waveguides will guide light around much smaller radii of curvature than planar guides can.

## Waveguide Measurements

To measure the performance of the waveguides, both ends of the substrates were polished to provide flat smooth input and output surfaces. We attached single mode fiber to the single leg of the "Y". The fiber was used to couple in light from a low power HeNe laser source. We observed the other end of the substrate with a CCD camera connected to an IBM PC computer. The computer generated three-dimensional plots of the light intensity as a function of position[9]. The patterns produced by both the ridge and planar waveguides were distinct, approximately Gaussian beam profiles. The waveguides successfully preserved the characteristics of the input laser beam, validating the fabrication techniques.

## Waveguide Lasers

We are currently fabricating single waveguide and coupled waveguide lasers for use in active optical circuits. The bandwidth of fiber communication, at present, is limited by the electro-optic input and output devices. Passive waveguide circuits can be used to multiplex low speed parallel electronic signals into high speed serial optical signals. Waveguide lasers can be used as optically activated optical switches in demultiplexing networks. These networks convert a high speed optical input to low speed parallel optical outputs that can then be detected by low speed electro-optic sensors.

Instead of passive optical quality glass, we used glass which was doped with active laser atoms such as Nd, Er, and Pr as the substrate material of the waveguide lasers. The first waveguide lasers are fabricated out of optical

quality Nd doped glass. The Ag doped waveguides are fabricated using the same technique as the glass waveguide. Both planar and ridge waveguides are being used. The lasers use external dielectric layered mirrors. Both devices with vertically polished ends and with ends that are polished at the Brewster angle are being fabricated. The Brewster angle laser ends provide less reflection by the boundary for polarized light than straight ends do. However, it is harder to attach mirrors to the Brewster angle faceted waveguides. The single waveguide lasers have a waveguide that has a slight S-curve to guide only low order modes. A planar waveguide laser is shown in Figure 9. Higher order modes will be radiated in the curving section of the waveguide.
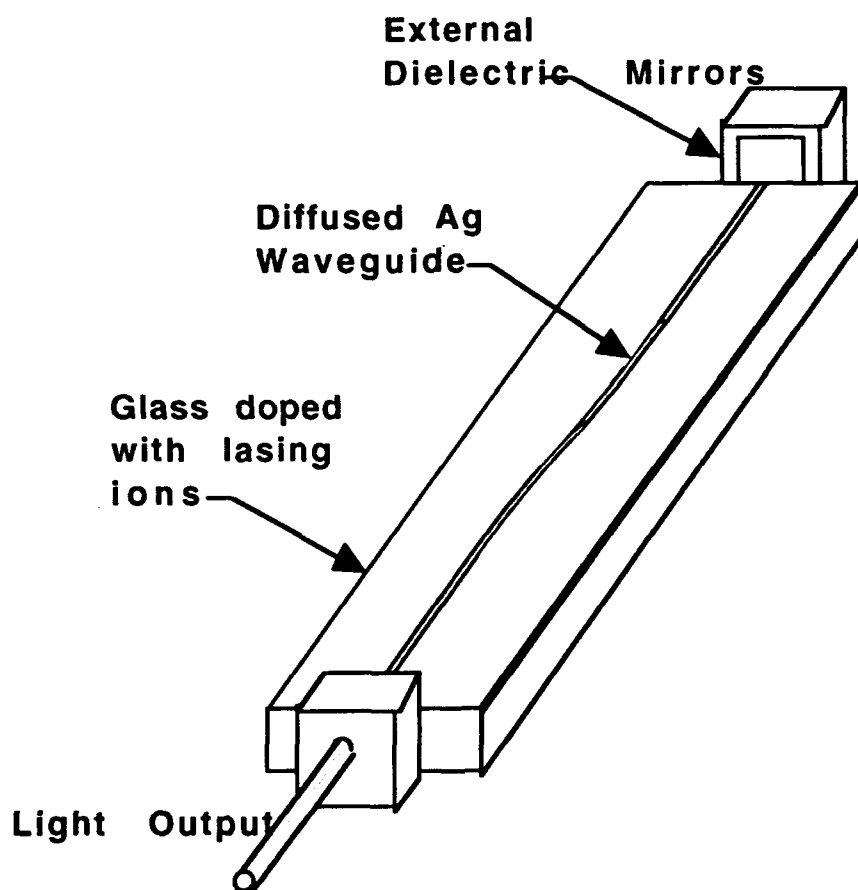
Figure 9. Single waveguide laser with external mirrors.

There are several methods of pumping these lasers. The first method we plan to use is to pump the waveguide lasers from the top as shown in Figure 10.

The substrate is illuminated from the top by a gas discharge lamp. In order to minimize heating of the waveguide laser, the light from the gas discharge lamp is dispersed by a prism. Light with different wavelength $\lambda$ is dispersed in different directions by the prism. A prism and a slit are used to select the appropriate pumping wavelength from the gas discharge lamp. Only the light with the desired wavelength for pumping passes through the slit and illuminates the waveguide. Light at other wavelengths is blocked by the shield.
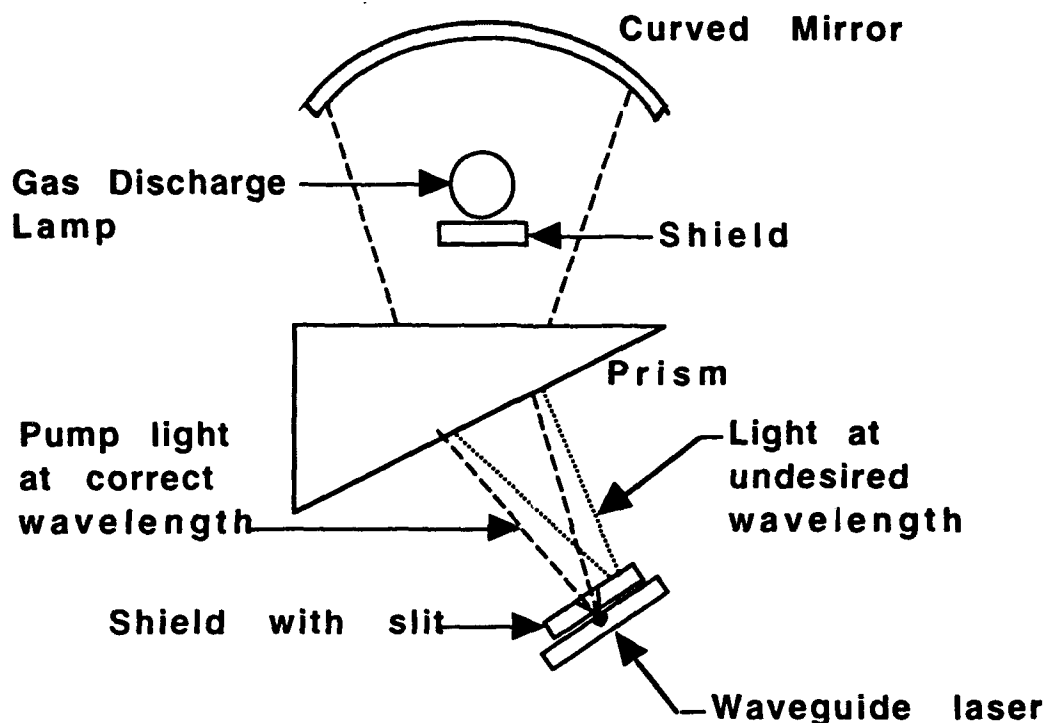


Figure 10. Laser pumping by direct illumination.

Another method of pumping the laser is to use a diode laser that radiates at the correct pumping wavelength. The light from the diode laser propagates collinearly with the signal light. The waveguide laser is illuminated through one of the dielectric mirrors. The dielectric mirrors only reflect light at the signal light wavelength, since they are relatively transparent at other wavelengths.

A third method of pumping the waveguide laser is to use a circular waveguide as a resonant laser cavity, as shown in Figure 11. This method eliminates the use of external mirrors. Only the counter clockwise mode will be amplified and will lase. The clockwise mode will be lost through the pumping

**Circular resonant cavity waveguide**

**Pump light input**

**Output light beam**

**Evanescent coupled output waveguide**

**Glass substrate doped with active lasing ions**
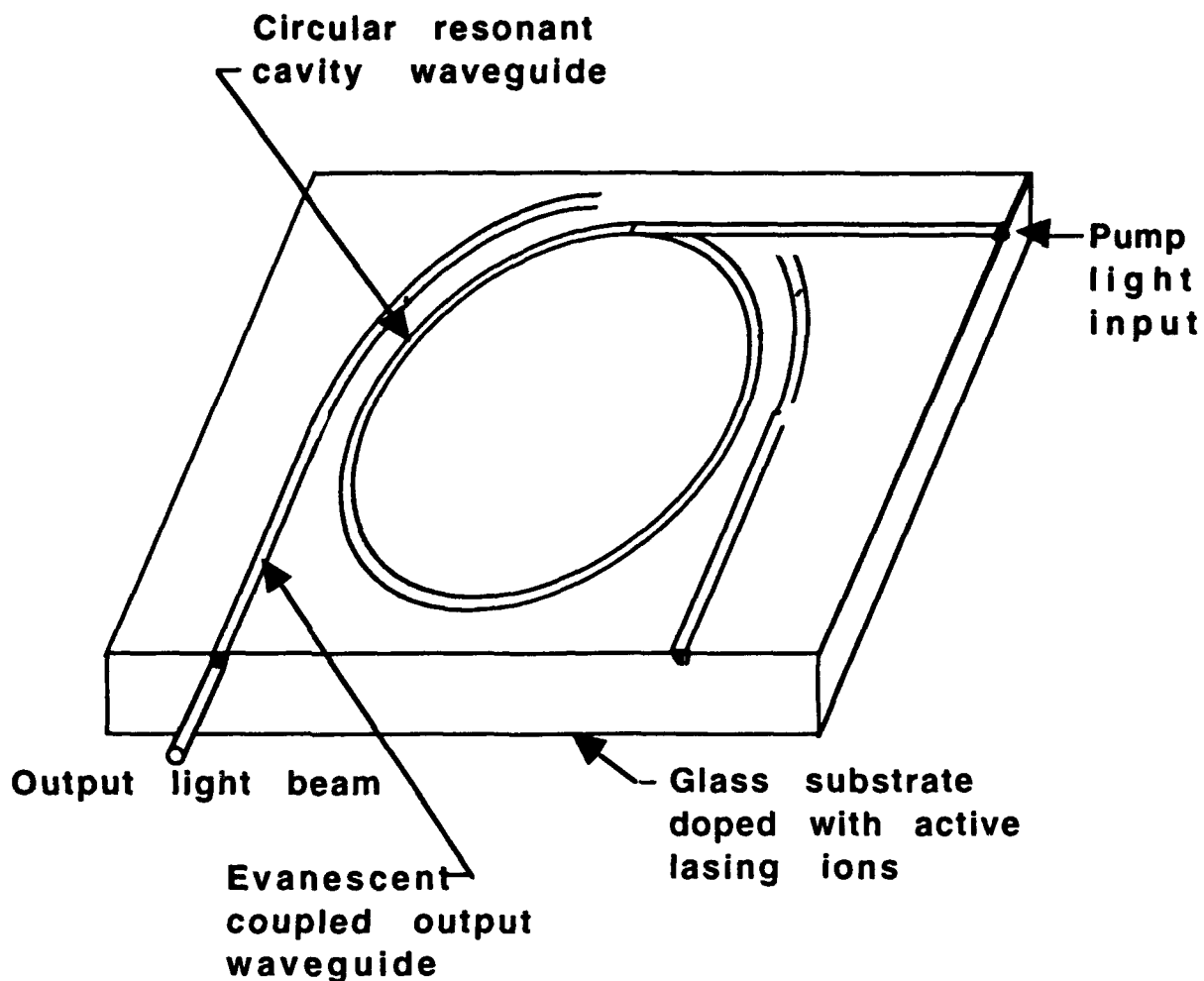
Figure 11. A circular waveguide used as a resonant cavity.

port. This device is designed to be pumped by a diode laser through the pumping port. The output from the laser is obtained through a waveguide that is evanescently coupled to the circular resonant waveguide cavity. This device would be fabricated using ridge waveguides rather than planar waveguides since the light has to be guided around a circle of only about 10 mm radius.

## Coupled Waveguide Lasers

Our ultimate goal is the fabrication and testing of coupled waveguide lasers. A Y-cavity coupled waveguide laser is shown in Figure 12. These devices have contacts so that an electric field can be applied across the waveguides. The wavelength of one of the outputs can be shifted with respect to the other output by the application of a voltage to the contacts. The application of an electric field across one of the waveguides shifts the energy levels of the active lasing ions in that waveguide. The shift of energy levels by an electric field is known as the Franz Keldish effect. The Franz Keldish effect shifts the gain curve of the laser branch that has a bias applied causing it to oscillate at a slightly different wavelength than the other branch of the laser.
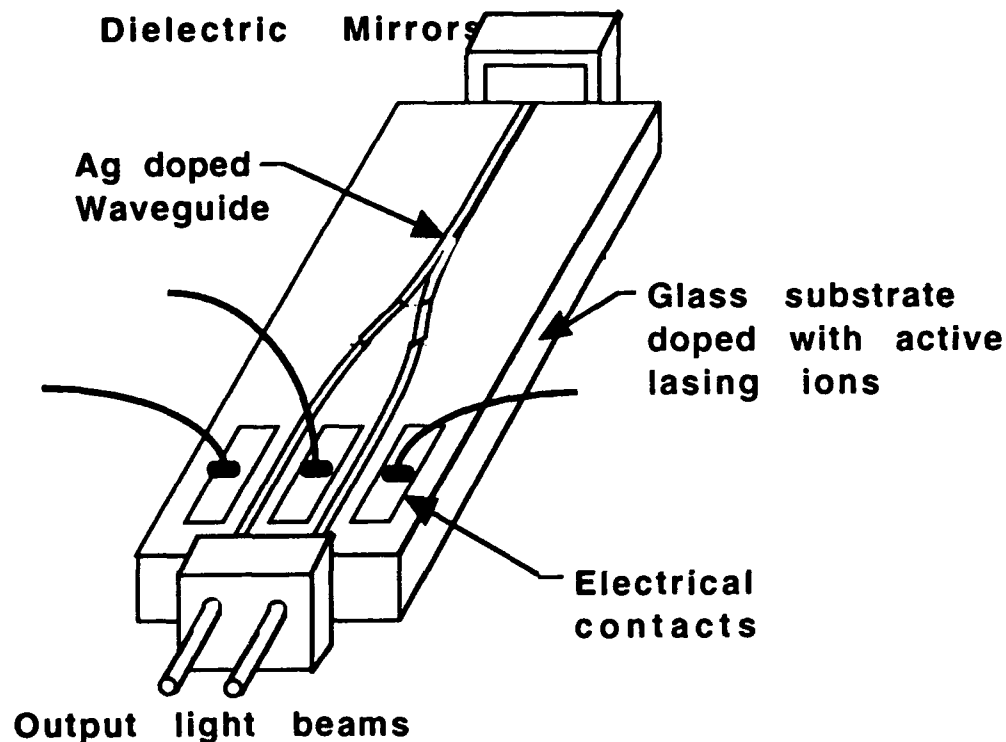
Figure 12. Y-type waveguide coupled lasers.

This device can be used in heterodyne optical processors where light waves differ in frequency by microwave or millimeter (mm) wave frequencies. This is often accomplished with acousto-optic cells. However, acousto-optic cells are limited to frequencies below about 1 GHz. The coupled lasers are theoretically able to provide frequency differences of up to about 100 GHz. The frequency difference is adjusted with the electrical bias applied across the waveguides.

Other configurations of coupled waveguide lasers are possible. One can, for example, use two evanescently coupled waveguides for this application.

## Artificial Optical Delay Line [10]

The Artificial Long Delay Optical Processor (ALDOP) generates a large variable delay of a band limited pulse modulated RF signal. The proposed prototype ALDOP has potential use in a Passive Radio Ranging (PRR) system operating in the 82.5-97.5 MHz frequency band. The complete system will combine a passive electronic band pass filter with the optically based ALDOP to impart a unique phase shift to each frequency component of an incoming RF signal. The phase shift is generated using optical heterodyne methods that incorporate the transmission and modulation of light through a series of optical components including an acousto-optical cell and a Fresnel Zone Plate.

### System Description

The generation of RF signals with long variable delays is difficult to achieve with great accuracy in purely electronic based systems. It has been demonstrated that optical systems are more suitable for achieving precise delays using *optical heterodyne techniques*[11]. One application of an ALDOP is in a prototype Passive Radio Ranging (PRR) system[12] that operates at 82.5-97.5 MHz. The corresponding fractional RF bandwidth of 16.667 % is centered at 90 MHz. This particular frequency range is chosen for two reasons: 1) local FM and TV broadcast stations provide convenient RF illumination of targets in this frequency range, and 2) acousto-optic (AO) cells driven by RF signals in the 62.5-77.5 MHz range are readily available. The corresponding fractional bandwidth of 21.429 % is centered at 70 MHz. The optical processor provides the 62.5-77.5 MHz broadband local oscillator (LO) for this system.

Consider a signal $S_1$ with $f_1 = 100$ MHz propagating a distance of 5 km from a target to an antenna, while a signal $S_2$ with $f_2 = 80$ MHz is traversing the same distance. The signals will undergo phase shifts of $\phi_1 = 10479.225$ radians for $S_1$ and $\phi_2 = 8383.380$ radians for $S_2$. The optical processor has to compensate for signals with phase shifts between $\phi_1$ and $\phi_2$.
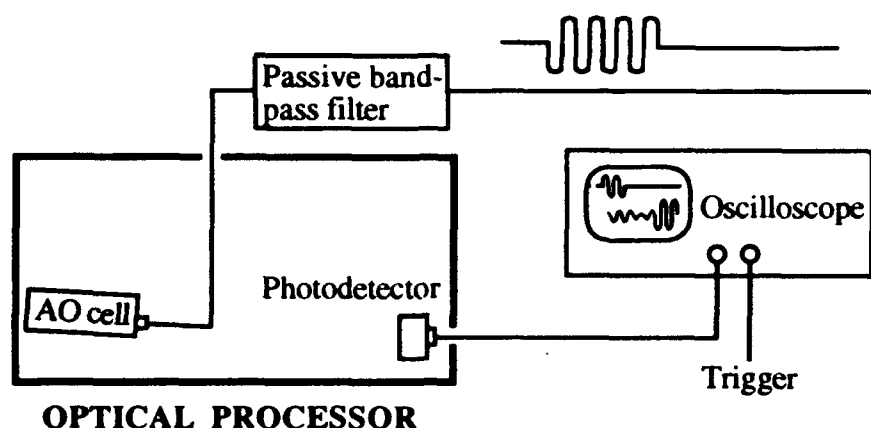
Figure 13. Schematic of the Artificial Long Delay Optical Processor.

The ALDOP functions as follows: a band limited electronic signal is produced by passing a periodic pulse modulated RF (or microwave) signal through a passive electronic band pass filter. The output is a continuous signal whose frequency components are limited by the pass band of the filter. The filter produces a signal for a time on the order of several milliseconds after the input pulse has ceased to exist. Therefore, the storage of the signal during the relatively long delay actually occurs within the filter. The output is used as the driving signal for an AO cell whose characteristic bandwidth and center frequency are matched to the filter.

## Optical Processor

The optical processor shown in Figure 14 utilizes the optical heterodyne techniques of Toughlian and Zmuda[11]. A HeNe laser beam is split by a non-polarizing beamsplitter into reference ($\omega_0$) and signal beams. The AO cell shifts the laser beam proportionally to the frequencies of the RF signal (filter output) which translates into an angular spread. The measured spread at the output of the IntraAction model AOD-70 AO cell used in this experiment was 2.4375 mRad (=0.139658°) for a bandwidth of 15 MHz centered at 70 MHz.
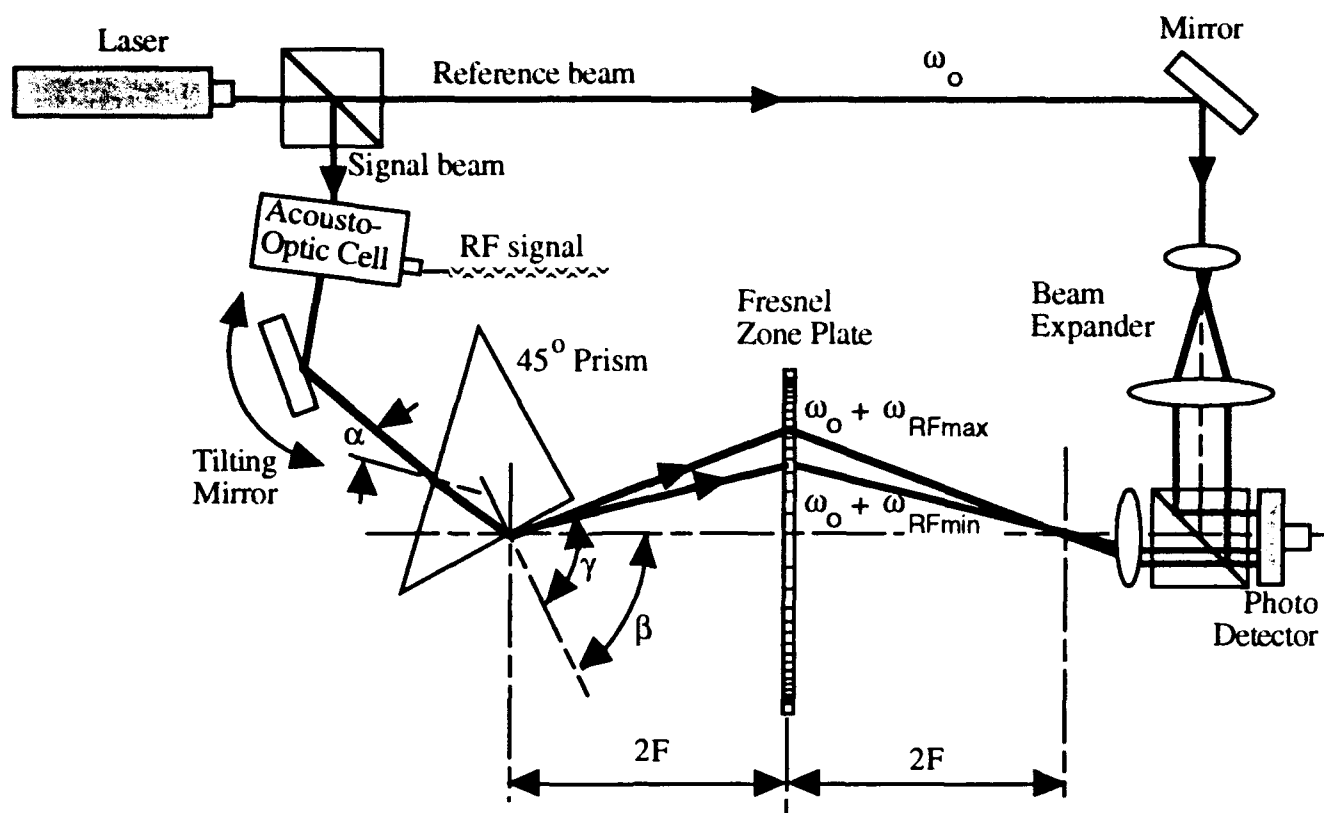
Figure 14. Detail of ALDOP.

The tilting mirror allows for adjustment of the incidence angle a of the light beam to the prism to vary the magnification of the angular spread of the light beam exiting the prism. A $45^\circ$ prism made from Schott BK-7 glass with an index of refraction n=1.51509 at $\lambda$=632.5 nm is used to increase the angular spread to a maximum of $1.279371^\circ$. Portions of the beam (denoted $\omega_0+\omega_{RFmax}$ and $\omega_0+\omega_{RFmin}$ in Figure 14) that are shifted by different RF drive frequencies will emerge at different angles from the prism.

A Fresnel Zone Plate (FZP) with a zero order focal length F is used to focus the spreading light beam. Different phase shifts are produced by the variation in optical path length through the FZP. The arrangement of the prism and FZP is designed to generate the largest phase shift of the light beam shifted by the highest RF frequency ($\omega_{RFmax}$).

Since the optical path length differences are large compared to light wavelengths, it is possible to obtain very large phase shift differences. Each beam incurs a phase shift $\phi(\omega_{RF})$ :

33

$$\phi(\omega_{RF}) = \frac{4F}{\lambda} \frac{1}{\cos(\gamma - \beta)} \qquad (1)$$

where $\beta$ is an offset angle and where we neglected the path from the AO cell to the output of the prism. We assume that the spread of the light beam from the AO cell is small compared to the spread of the light beam after the prism. The output angle $\gamma$ is related to the incident angle $a$ of the prism input beam by the following relation:

$$\sin\gamma = \frac{1}{\sqrt{2}} \left[ \sqrt{n^2 - \sin^2\alpha} - \sin\alpha \right] \qquad (2)$$

The angle $\alpha$ is related to the exit angle $\gamma$ of the prism output beam by a similar relation:

$$\sin\alpha = \frac{1}{\sqrt{2}} \left[ \sqrt{n^2 - \sin^2\gamma} - \sin\gamma \right] \qquad (3)$$

In both equations, n is the index of refraction. The largest magnification of the angular spread by the prism will occur when $\gamma = 90°$, corresponding to an incident angle $\alpha_0 = 5.608°$. The prism is adjusted in such a way that when the tilting mirror is at the maximum gain position, the light beam shifted by the largest signal frequency $(\omega_0 + \omega_{RFmax})$ emanates from the prism with an angle $\gamma = 90°$.

The delay $\tau = \dfrac{d\phi(f_{RF})}{df_{RF}}$ is the change of the phase $\phi(f_{RF})$ with frequency $f_{RF}$ One can obtain an expression for $\tau$ by substituting eq. (2) for $\gamma$ into eq. (1) and differentiating the resulting expression with respect to the frequency $f_{RF}$.

$$\tau = \frac{4F}{\lambda} \frac{\sin(\gamma - \beta)}{\cos^2(\gamma - \beta)} \frac{\sin\gamma\cos\alpha}{\cos\gamma} \frac{1}{\sqrt{n^2 - \sin^2\alpha}} \frac{d\alpha}{df_{RF}} \qquad (4)$$

where

$$\alpha = \alpha_0 + \alpha_{mirror} \qquad (5)$$

34

with $\alpha_{Mirror}$ defined as the tilt angle of the mirror. The IntraAction AO cell has a $\frac{d\alpha}{df_{RF}} = 1.625 \times 10^{-10}$ Rad-sec (Rad per Hz). A theoretically calculated plot of $\tau$ as a function of $\alpha_{Mirror}$ for $\beta = 84.5°$ is shown in Figure 15. It is possible to obtain a delay $\tau$ ranging from approximately 10-400 µsec corresponding to a change in tilt angle $\alpha_{Mirror}$ from 0.25° to 0.0 °.
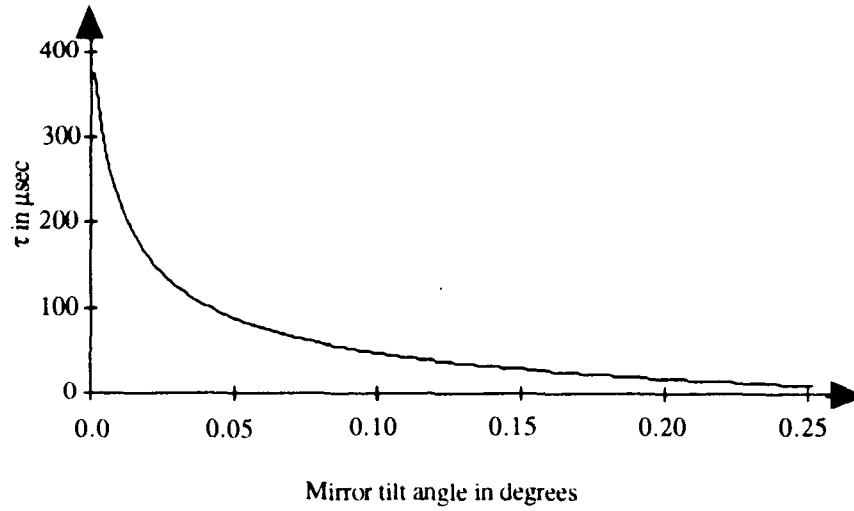


Figure 15. Calculated plot of the delay $\tau$ ( $\alpha$)

**Impulse Response**

The impulse response of the ALDOP system can be obtained by considering a train of impulses $g(t)$ of period T, given by:

$$g(t) = \sum_{n=-\infty}^{n=\infty} \delta(t - nT) \tag{6}$$

The Fourier transform of $g(t)$ gives the equivalent expression for the impulse train in the frequency domain as:

$$G(\omega) = \sum_{n=-\infty}^{n=\infty} e^{-j\omega nT} \tag{7}$$

35

Each frequency component is shifted by a phase $\omega\tau$ proportional to the frequency $\omega$ :

$$H(\omega) = \sum_{n=-\infty}^{n=\infty} e^{-j\omega(nT - \tau)}$$

(8)

By taking the band limited inverse Fourier transform we obtain:

$$h(t) = \frac{1}{2\pi}\int_{\omega_c\left(1-\frac{B_w}{2}\right)}^{\omega_c\left(1+\frac{B_w}{2}\right)} d\omega \sum_{n=-\infty}^{n=\infty} e^{-j\omega(nT - \tau - t)}$$

(9)

where $\omega_c$ is the center frequency of the bandwidth $B_w$. Evaluating the integral of Eq. 9 yields the transfer function $h(t)$ of the Artificial Long Delay Optical Processor :

$$h(t) = \frac{\omega_c B_w}{2\pi}\sum_{n=-\infty}^{n=\infty} \frac{\sin\frac{\omega_c B_w}{2}(nT - \tau - t)}{\frac{\omega_c B_w}{2}(nT - \tau - t)} e^{-j\omega_c(nT-\tau-t)}$$

(10)

where $\tau$ is the delay generated by the optical processor (see Eq. 4). Indeed, it should be possible to obtain delays as large as 400 $\mu$sec, corresponding to a detection range of 119.916 kilometers for the PRR system.

## Conclusions and Recommendations

### FLC Spatial Light Modulator

The tests of the individual elements and the entire SLM array demonstrate how the device has not been optimized for operation at 1320 nm. The data from the elements that were tested suggest that the optic axis fails to switch 45 degrees when the voltage is switched. Investigation of the dependence of the rotation of the optic axis on the voltage supplied to the elements may reveal that the voltage being applied has not been optimized for operation at 1320 nm. Another factor that needs to be investigated is the dependence of the thickness of the FLC layer on the switching of the optic axis. The current thickness may not be ideal for 1320 nm light.

The overall assessment of the SLM was that it is not optimal for the intended application where it would be used to independently switch 25 spatially separated laser beams. The switching requirement would easily be satisfied by the manufacturer's design of the controller, driver, and software, but the need to rotate the array to maximize the throughput for each element disqualifies the array as a candidate for the modulation of the low power laser beams in the system. The variation in contrast ratio among individual pixels at a fixed angle indicates that the throughput of some elements would not be maximized without rotation of the array. The SLM is generally used with a laser beam of sufficient power so that the reduced throughput would not adversely affect the dynamic range of a detection system. In this application, the decreased throughput that will result in the pixels that are not oriented at their maximum would cause detection of the low power laser beams to be close to the noise level of a photodetector.

### Active Optical Waveguide Circuits

Dr. Kornreich is currently pursuing the development of waveguide laser-based active optical circuits. This technology seems to offer more possibilities than was anticipated when this task started. As previously stated, one of the main limitations of the speed by which data can be transmitted over optical

fibers is the relatively slow response of electronic circuits. Electronic light modulators and detectors are currently limited to about 20 to 30 GHz while optical fibers have a bandwidth of $10^{14}$ Hz. Active optical circuits using coupled waveguide lasers can, theoretically, switch in about 50 fsec. Such devices can be used to convert 'slow' parallel electronically generated optical signals to 'fast' serial optical signals that are then transmitted over a fiber. The high speed serial optical signals from the fiber are then converted to lower speed optical parallel signals using active waveguide circuits. The low speed optical parallel signals can than be detected electronically. Dr. Kornreich hopes to have an active waveguide circuit working by the end of 1993. The work started here was transferred to another in-house project for the remainder of FY93.

For some time people were trying to fabricate light emitting devices on silicon Integrated Circuits (ICs). Several approaches have been tried. One approach is to mount light emitting devices made out of other semiconductors such as GaAs on silicon ICs. However this is a very tedious process. Another approach is to fabricate light emitters in the silicon itself. This requires very high current densities which result in large power consumption and high temperatures.

Fabrication of optical waveguide circuits on silicon ICs has recently been proposed (not by Syracuse University). Such devices can be fabricated by Chemical Vapor Deposition (CVD) processes on silicon substrates. The CVD process differs little from other CVD processes already in use in silicon IC fabrication. The fabrication of optical waveguide circuits on silicon ICs for the first time allows the integration of the highly developed silicon technology with high speed active optical circuits. Dr. Kornreich highly recommends that the active optical waveguide circuit technology be further developed.

## Electro-Optic Tunneling Devices

The results of the work with the various Metal-Oxide-Metal tunneling devices was less successful. Even though this technology is theoretically promising, it was not possible to construct useful devices to date. It is Dr. Kornreich's opinion that there is no fundamental theoretical limitation that states that such devices could never be produced. While working with the tunneling

devices it was concluded that a substantially larger effort than this program allowed would be required to achieve any success. The light assisted tunneling transistor is an interesting device. This technology will require much more research before any practical devices can be fabricated.

## Artificial Optical Delay Line

The work with the Artificial Optical Delay Line was hampered by an extensive time lag in the delivery of the Fresnel Zone Plate. The experiment was continued on a part-time basis by Dr. Kornreich. The technical paper describing the ongoing work is currently in progress and should be released by the end of the summer of 1993. It is not recommended that this work be continued under the branch in-house efforts. The proof of concept was realized but did not meet expectations.

# References

[1] C.L. Wang, J.T. Tung, J.D. Smith and P. Kornreich, "CdTe-InSb nonlinear etalon switch",*SPIE Proceedings,* Vol. 1790, pp 126-9, Sept 1992.

[2] P. L. Gouley and T. J. Drummond, "Optical bleaching in an epitaxial (Al, Ga) As Fabry-Perot Resonator," *Appl. Phys. Lett.,* Vol. 51, pp. 1395-1397, 1987.

[3] T. H. Wood, C.A. Burrus, D.A.B.Miller, D. S. Chemla, T. C. Damen, A. C. Gossard and W. Wiegmann, "131 ps optical modulation in semiconductor multiple quantum wells", *IEEE Jour. of QE,* Vol. QE-21, pp. 117-118, 1985.

[4] D. A. B. Miller, D. S. Chemla, T. C. Damen, T. H. Wood, C.A. Burrus, Jr., A. C. Gossard, ar J W. Wiegmann, "The quantum well self-electrooptic effect device: Optoelectronic bistability and oscillation, and self-linearized modulation", *IEEE Jour. of QE,* Vol. QE-21, pp. 1462-1476, Sept. 1985.

[5] A. L. Lentine et al., "Multistate self-electrooptics effect devices", *IEEE Jour. of QE,* Vol. QE-25, pp1921-1927, Aug. 1989.

[6] D. Stanchfield and J.D.Smith, "Measurement of Contrast Ratios for a Ferroelectric Liquid Crystal Spatial Light Modulator", 1993, publication pending.

[7] D. Stanchfield, P.G. Kornreich, J.D. Smith, Measurement of Contrast Ratios for a Ferroelectric Liquid Crystal Spatial Light Modulator, Rome Laboratory technical report # RL-TR-91-404, Air Force Systems Command, Griffiss Air Force Base, NY 13441-5700. Dec 1991.

[8] P.G. Kornreich, "Analysis of Devices for Pulse Position Modulation Networks", Final Report, publication pending : Rome Laboratory technical report, Air Force Materiel Command, Griffiss Air Force Base, NY 13441-5700. Dec 1991.

[9] See Figures 3 and 4 of Reference 8.

[10] P.G. Kornreich, J.D. Smith, Artifical Long Delay Optical Processor, SPIE Proceedings, Vol. 1790, pp 130-2, Sept 1992.

[11] E. Toughlian and H. Zmuda, "A Photonic Variable RF Delay Line for Phased Array Antennas", *IEEE Journal of Lightwave Technology,* Vol. 8, No. 12, pp. 1824-1828, 1990.

[12] N.H. Farhat, "Principles of Broad-Band Coherent Imaging", *Journal of the Optical Society of America,* Vol. 67, No. 8, pp. 1015-1021, August 1977.

## *MISSION*

## *OF*

## *ROME LABORATORY*

Rome Laboratory plans and executes an interdisciplinary program in research, development, test, and technology transition in support of Air Force Command, Control, Communications and Intelligence (C3I) activities for all Air Force platforms. It also executes selected acquisition programs in several areas of expertise. Technical and engineering support within areas of competence is provided to ESC Program Offices (POs) and other ESC elements to perform effective acquisition of C3I systems. In addition, Rome Laboratory's technology supports other AFMC Product Divisions, the Air Force user community, and other DOD and non-DOD agencies. Rome Laboratory maintains technical competence and research programs in areas including, but not limited to, communications, command and control, battle management, intelligence information processing, computational sciences and software producibility, wide area surveillance/sensors, signal processing, solid state sciences, photonics, electromagnetic technology, superconductivity, and electronic reliability/maintainability and testability.